

Crucial roles of eastward propagating environments in the summer MCS initiation over the U.S. Great Plains

Fengfei Song¹, Zhe Feng², L. Ruby Leung³, Binod Pokharel⁴, Shih-Yu (Simon) Wang⁴, Xingchao Chen⁵, Koichi Sakaguchi², and Chi-Chia Wang⁶

¹Pacific Northwest National Laboratory

²Pacific Northwest National Laboratory (DOE)

³PNNL

⁴Utah State University

⁵Pennsylvania State University

⁶Central Weather Bureau

November 22, 2022

Abstract

This study aims at improving understanding of the environments supporting summer MCS initiation in the U.S. Great Plains. A self-organizing map analysis is conducted to identify four types of summer MCS initiation environments during 2004-2017: Type-1 and Type-2 feature favorable large-scale environments, Type-3 has favorable lower-level and surface conditions but unfavorable upper-level circulation, while Type-4 features the most unfavorable large-scale environments. Despite the unfavorable large-scale environment, convection-centered composites reveal the presence of favorable sub-synoptic scale environments for MCS initiation in Type-3 and Type-4. All four types of MCS initiation environments delineate a clear eastward propagating feature in many meteorological fields, such as potential vorticity, surface pressure and equivalent potential temperature, upstream up to 25 west of and ~36 hours before MCS initiation. While the propagating environments and local, non-propagating low-level moisture are important to MCS initiation at the foothill of the Rocky Mountains, MCS initiation in the Great Plains is supported by the coupled dynamical and moisture anomalies, both associated with eastward propagating waves. Hence, the MCSs initiated at the plains can produce more rainfall than those initiated at the foothill due to more abundant moisture supply. By tracking MCSs and mid-tropospheric perturbations (MPs), a unique type of sub-synoptic disturbances with Rocky Mountains origin, it is shown that ~30% of MPs is associated with MCS initiation, mostly in Type-4. Although MPs are related to a small fraction of MCS initiation, MCSs that are associated with MPs tend to produce more rainfall in a larger area with a stronger convective intensity.

1 **Crucial roles of eastward propagating environments in the summer**

2 **MCS initiation over the U.S. Great Plains**

3 Fengfei Song¹, Zhe Feng¹, L. Ruby Leung¹, Binod Pokharel², S.-Y. Simon Wang², Xingchao
4 Chen³, Koichi Sakaguchi¹, and Chichia Wang^{2,4}

5 1. Atmospheric Sciences and Global Change Division, Pacific Northwest National Laboratory,
6 Richland, Washington, USA

7 2. Department of Plants, Soils, and Climate / Utah Climate Center, Utah State University, Logan,
8 Utah, USA

9 3. Department of Meteorology and Atmospheric Science, and Center for Advanced Data
10 Assimilation and Predictability Techniques, The Pennsylvania State University, PA, USA

11 4. Central Weather Bureau, Taipei, Taiwan

12

13

14 Submitted to *Journal of Geophysical Research: Atmospheres*

15

16

17

18 **Corresponding author:**

19 Fengfei Song (Fengfei.Song@pnnl.gov)

20 **Key points:**

21 1. Summer MCSs in the U.S. Great Plains can initiate under unfavorable large-scale
22 environments when favorable sub-synoptic forcing is present.

23 2. It propagates eastward for both large-scale and sub-synoptic environments, up to 25° west of
24 and 36 hours prior to the MCS initiation.

25 3. About 30% of MPs from the Rocky Mountains are related to the initiation of intense MCSs
26 under weak large-scale forcing.

27

Abstract

28 This study aims at improving understanding of the environments supporting summer
29 MCS initiation in the U.S. Great Plains. A self-organizing map analysis is conducted to identify
30 four types of summer MCS initiation environments during 2004-2017: Type-1 and Type-2
31 feature favorable large-scale environments, Type-3 has favorable lower-level and surface
32 conditions but unfavorable upper-level circulation, while Type-4 features the most unfavorable
33 large-scale environments. Despite the unfavorable large-scale environment, convection-centered
34 composites reveal the presence of favorable sub-synoptic scale environments for MCS initiation
35 in Type-3 and Type-4. All four types of MCS initiation environments delineate a clear eastward
36 propagating feature in many meteorological fields, such as potential vorticity, surface pressure
37 and equivalent potential temperature, upstream up to 25° west of and ~36 hours before MCS
38 initiation. While the propagating environments and local, non-propagating low-level moisture are
39 important to MCS initiation at the foothill of the Rocky Mountains, MCS initiation in the Great
40 Plains is supported by the coupled dynamical and moisture anomalies, both associated with
41 eastward propagating waves. Hence, the MCSs initiated at the plains can produce more rainfall
42 than those initiated at the foothill due to more abundant moisture supply. By tracking MCSs and
43 mid-tropospheric perturbations (MPs), a unique type of sub-synoptic disturbances with Rocky
44 Mountains origin, it is shown that ~30% of MPs is associated with MCS initiation, mostly in
45 Type-4. Although MPs are related to a small fraction of MCS initiation, MCSs that are
46 associated with MPs tend to produce more rainfall in a larger area with a stronger convective
47 intensity.

48

Plain Language Summary

49 During warm season (spring and summer), MCSs are often observed over the U. S. Great
50 Plains and contribute considerably to the seasonal mean rainfall. However, compared to spring,
51 the summertime MCS initiation is poorly understood, as large-scale environments are
52 substantially weakened and the smaller-scale forcing is difficult to estimate based on the coarse-
53 resolution observations. Here, we use newly-developed MCS tracking dataset and newly-
54 released ERA5 reanalysis dataset, both having high spatialtemporal resolutions to examine the
55 summertime MCS initiation environments. We find that the eastward propagating environments
56 at both large and smaller spatial scales, which can exist several days before the MCS initiation,
57 play a crucial role in the MCS initiation. Both the propagating environments and local moisture
58 are important for the MCS initiation at the foothill of Rocky Mountains, but at the central plains,
59 the MCS initiation are associated with the propgating environments by coupling moisture and
60 dynamical anomalies. Hence, the MCS rainfall is larger at the beginning several hours for those
61 initiated at the plains compared to those initiated at the foothill due to more moisture supply.
62 Finally, we quantify the contribution from one unique smaller-scale disturbances with Rocky
63 Mountains origin to the summer MCS initiation.

64 **1. Introduction**

65 During the warm season (spring and summer), mesoscale convective systems (MCSs) are
66 common features over the U.S. Great Plains (Houze, 2004, 2018; Schumacher & Rasmussen,
67 2020) and contribute substantially to the seasonal-mean and extreme rainfall (Feng et al., 2016,
68 2019; Fritsch et al., 1986; Nesbitt et al., 2006; Maddox et al., 1979; Schumacher & Johnson,
69 2005, 2006; Haberlie & Ashley, 2019). The role of synoptic environments in the warm-season
70 MCS initiation has been extensively studied. Warm season MCSs are often initiated ahead of
71 large-scale troughs at the upper troposphere with positive vorticity advection (e.g., Maddox,
72 1983; Anderson & Arritt 1998; Coniglio et al. 2004; Yang et al. 2017; Song et al., 2019) or
73 beneath the upper-level ridge (e.g., Coniglio et al. 2004; Song et al. 2019), on the warm side of a
74 synoptic front at the surface (e.g., Peters & Schumacher, 2014; Coniglio et al. 2010; Song et al.
75 2019), and/or at the exit region of the Great Plains low-level jet (GPLLJ) that converges moisture
76 and destabilizes the atmosphere (e.g., Maddox, 1983; Anderson & Arritt 1998; Laing & Fritsch,
77 2000; Coniglio et al., 2010; Song et al. 2019).

78 However, compared to spring, synoptic forcing is considerably weaker so it plays a
79 smaller role in summer MCS development (Song et al., 2019), which suggests a more important
80 role of other forcings contributing to the development of summer MCSs. Our limited
81 understanding of those forcings has implications, as summer MCSs are also more difficult to
82 simulate and predict (Gao et al., 2017; Yang et al., 2017; Feng et al., 2018, 2021; Prein et al.,
83 2020). Despite the weaker synoptic forcing, MCS intensity and precipitation amount can be
84 stronger during summer than spring as noted by Feng et al. (2019), potentially posing larger
85 threats of derechos, hails, tornadoes and flash flooding. Hence, there is an urgent need to
86 improve our understanding on factors that contribute to the summertime MCS initiation.

87 Most previous studies did not distinguish the large-scale environments of MCSs between
88 spring and summer over the Great Plains, but some studies noticed that summertime MCSs
89 frequently occur under northwesterly flow associated with a high-pressure ridge to the west and a
90 low-pressure trough to the east (e.g., Johns, 1982, 1984, 1993; Carbone et al., 2002; Wang et al.,
91 2011a, b; Pokharel et al., 2019). Such large-scale environment is commonly thought to be
92 unfavorable for MCS initiation due to the anticyclonic circulation aloft and the prevailing
93 negative vorticity advection. Instead, sub-synoptic perturbations such as eastward-propagating
94 waves (Li & Smith, 2010), residual short-wave troughs (Tuttle & Davis, 2013) and mid-
95 tropospheric perturbations (MPs; Wang et al., 2011a, b; Pokharel et al., 2019), which appear to
96 be embedded in the large-scale westerly or northwesterly flow, may support MCS initiation.

97 Using self-organizing map (SOM) analysis, Song et al. (2019) found a similar amount of
98 summer MCS initiation in the U.S. Great Plains under either favorable or unfavorable large-scale
99 environments. However, our current understanding on the role of sub-synoptic perturbations in
100 the summertime MCS initiation is still limited, as it requires datasets with high spatiotemporal
101 resolution. Using the North American Regional Reanalysis 32-km-resolution and 3-hourly data
102 (NARR; Mesinger et al., 2006), Wang et al. (2011a, b) tracked MPs that originate from the
103 Rocky Mountains and found that MPs exhibit a diurnal distribution with a primary peak at 12
104 UTC (early morning) and a secondary peak at 00 UTC (late afternoon). The early morning peak
105 is linked to the lee side vorticity generation in the mid-troposphere, while the late afternoon peak
106 is linked to a Charney-Stern type of instability in the mid-troposphere of the Rocky Mountains.
107 As discussed by Wang et al. (2011a), the potential vorticity (PV) associated with the sub-
108 synoptic scale perturbations are notably different from the PV generated by mature MCSs, which
109 has an average wavelength around 400 km, much shorter than the sub-synoptic scale

110 perturbations with wavelength ranging from 700 to 1500 km. Wang et al. (2011a) also found that
111 up to 60% of rainfall and storm reports over the northern plains in July and August could be
112 associated with the presence of MPs. However, to what extent MPs are connected to organized
113 storms like MCSs is not clear. Tuttle & Davis (2013) produced a 10-year (1998-2007)
114 climatology of eastward traveling short waves with a wavelength of 1500 km using NARR and
115 found that some of the short waves can be traced back to the Pacific Northwest as residual
116 synoptic waves (Trier et al., 2006), which are different from the MPs that originate mainly from
117 the Rocky Mountains. These studies suggested that short waves only play a secondary role in the
118 diurnal cycle of precipitation over the Great Plains, as the latter is functional regardless of the
119 presence of a short wave. Nonetheless, propagating short waves or other sub-synoptic
120 perturbations connected to MCS initiation may provide a source of predictability for MCSs in the
121 Great Plains. As MCSs contribute substantially to the diurnal cycle of precipitation, which
122 represents a major challenge in climate modeling (e.g., Lin et al., 2017; Ma et al., 2018; Feng et
123 al., 2021), it is important to quantify the relative contributions from different sources of sub-
124 synoptic perturbations to summer MCS initiation for improving prediction and simulation of
125 summertime MCSs in the U.S. Great Plains.

126 Taking advantage of high spatiotemporal MCS and MP tracking datasets and reanalysis
127 products that have become available in recent years, this study aims at furthering our
128 understanding of the large-scale vs. sub-synoptic scale environments supporting summer MCS
129 initiation in the U.S. Great Plains. To examine the role of large-scale environment vs. sub-
130 synoptic perturbations in MCS initiation, we use hourly MCS tracks (Feng 2019) and
131 hourly/0.25° ERA5 reanalysis (Hersbach et al., 2020) to develop a 14-year (2004-2017)
132 climatology of summertime MCS initiation environments and investigate their time evolution

133 before/after the MCS initiation. We also quantify the contribution of MPs to MCS initiation by
134 analyzing hourly MP tracks in combination with hourly MCS tracks. The remainder of this paper
135 is organized as follows: Section 2 introduces the MCS and MP tracking methods, the ERA5
136 reanalysis and our analysis methods. Section 3 discusses the main results, which include a
137 comparison between large-scale composite and convection-centered composite, vertical structure
138 of convection-centered environments, propagating features of convection-centered environments
139 and the role of MPs in MCS initiation. Section 4 provides a summary and discussions.

140 **2. Observational datasets and analysis methods**

141 Here, we focus on June-July-August (JJA) of 2004-2017 for MCS and MP tracking and
142 the use of the ERA5 reanalysis for the MCS environments.

143 **2.1 MCS tracking**

144 The MCS tracking dataset used here has hourly temporal resolution and 4 km spatial
145 resolution (Feng 2019) based on MCS tracking using the FLEXible object TRackER
146 (FLEXTRKR) algorithm (Feng et al., 2018) applied to three operational datasets: (1) a global
147 merged geostationary satellite infrared brightness temperature (T_b) data produced by National
148 Oceanic and Atmospheric Administration (NOAA) Climate Prediction Center (Janowiak et al.,
149 2017); (2) a 3-dimensional mosaic National Weather Service Next-Generation Radar
150 (NEXRAD) radar reflectivity data known as GridRad (Homeyer & Bowman 2017; Cooney et al.,
151 2018); and 3) the Stage IV multi-sensor hourly precipitation dataset produced by the 12 River
152 Forecast Centers in the continental United States (CONUS, Lin et al., 2011). The tracking
153 algorithm first identifies large cold cloud systems with brightness temperature less than 241 K,
154 then further identifies MCSs from these large cold cloud systems based on the radar reflectivity
155 data and precipitation data. An MCS is defined as a cold cloud system greater than 6×10^4 km²,

156 containing a precipitation feature with major axis length greater than 100 km, a convective
157 feature with radar reflectivity greater than 45 dBZ at all vertical levels, and precipitation feature
158 persisting for at least 6 h (Feng et al. 2019). Compared to other MCS tracking methods, which
159 use either cloud (e.g., Huang et al. 2018) or precipitation features (e.g., Stein et al. 2014) to
160 define MCSs, our method uses both the cloud and precipitation features to define MCSs, which
161 is more stringent and should be more accurate. Since the MCS tracking dataset uses satellite T_b ,
162 MCS lifecycle includes initiation of isolated convection that eventually grow upscale into MCSs.
163 MCS initiation in this study refers to the first hour of convection detected ($T_b < 241$ K) prior to
164 the formation of a mesoscale precipitation feature (> 100 km). See Feng et al. (2019) and Song et
165 al. (2019) for more details of the MCS tracking methods and MCS features.

166 **2.2 MP tracking**

167 MPs refer to the mid-tropospheric, sub-synoptic scale vortices that are embedded in the
168 northwesterly flow. They are generated over the Rocky Mountains and propagate across the
169 northern plains in the form of serial short-wave perturbations (Wang et al., 2011a, 2011b;
170 Pokharel et al., 2019). Using the hourly ERA5 reanalysis data, the criteria applied to track and
171 define MPs under the northwesterly background flows are modified from Pokharel et al. (2019)
172 that used 3-hourly NARR data. Three criteria are used to select MPs: first, cases with large-scale
173 upper-level troughs or low pressure are excluded; second, only cases with upper-level wind
174 speed greater than 15 m s^{-1} are considered, as prevailing westerly wind plays an important role in
175 the propagation of MPs; third, only cases with high precipitable water (>24 mm) are considered,
176 as dry vortices (e.g., Davis et al., 2002) do not generate severe weather outbreaks (Wang et al.
177 2011a, 2011b). In addition to these three criteria, a given MP should last for at least 12

178 continuous hours. See Pokharel et al. (2019) for more details of the MP tracking methods and
179 MP features.

180 **2.3 ERA5 reanalysis datasets**

181 We also use the following hourly variables from ERA5 (Hersbach et al., 2020) with 0.25°
182 and hourly resolution to conduct SOM analysis and a composite analysis: vertical velocity,
183 geopotential height, temperature and specific humidity at all levels; zonal and meridional wind at
184 200 hPa, 500 hPa and 925 hPa; potential vorticity (PV) at 200 hPa; surface pressure, surface air
185 temperature and dew-point temperature to calculate the surface equivalent potential temperature
186 (θ_e).

187 **2.4 Self-organizing map (SOM) analysis and composite methods**

188 Similar to Song et al. (2019), SOM analysis is conducted to identify four types of large-
189 scale environments associated with summertime MCS initiation over the Great Plains. Here, we
190 select the zonal and meridional winds at three levels (925, 500 and 200 hPa) and the specific
191 humidity at two levels (925 and 500 hPa) over the domain (20°-55°N, 70°-110°W) at the time of
192 MCS initiation to conduct the SOM analysis. As we focus on the environments conducive to
193 MCS development, only the environment variables at the time of MCS initiation are composited
194 to minimize the confounding effects of MCS on the large-scale environment. MCS initiation is
195 defined as the first hour that an MCS cold cloud ($T_b < 241$ K) is detected (Feng et al., 2018,
196 2019). All variables are normalized by removing their time mean and dividing by their standard
197 deviation over all MCS initiation times. A cosine latitude weighting is applied when the spatial
198 dimensions of the variables are collapsed into a single dimension.

199 To run SOM, the initiation nodes are assigned by randomly or more efficiently selecting
200 them from the leading empirical orthogonal functions. Then we calculate the Euclidean distance
201 between each input pattern and the initiation nodes to start an iterative procedure. The best-
202 matching node or the “winning” node is the one with the shortest distance between the initiation
203 nodes and the input pattern. Finally, the winning node and neighborhood nodes around the
204 winner are updated to adjust themselves toward the input pattern. Since this process is iterated
205 and fine-tuned by the inputs themselves, we call the nodes are self-organizing. The final SOM
206 nodes are regarded as the large-scale environment types associated with MCSs. More details
207 about the SOM analysis can be found from Song et al. (2019).

208 Here, we highlight the main differences from Song et al. (2019): (1) as the temporal
209 resolution of the MCS track data and ERA5 reanalysis are both hourly, we can composite the
210 environments at exactly the same time as the MCS initiation, but Song et al. (2019) had to
211 reconcile the different temporal resolution between NARR (3-hourly) and the MCS track data
212 (hourly); (2) Song et al. (2019) only adopted the fixed-space (Eulerian) compositing approach to
213 focus on the large-scale environments, but here we also adopt the convection-centered
214 (Lagrangian) compositing in addition to the fixed-space compositing to reveal the role of sub-
215 synoptic perturbations in MCS initiation; (3) to conduct the composite analysis, Song et al.
216 (2019) removed the seasonal mean, while here we first remove the 14-year averaged seasonal
217 mean diurnal cycle to remove the impact of climatological diurnal cycle, followed by removing
218 the five-day running mean to remove the impact of sub-seasonal variability. For example,
219 August temperature is generally higher than that in June, so without removing the five-day
220 running mean, MCSs that occur in August will be given more weighting on temperature and its

221 related fields, such as moisture. However, it is found that both methods show quite similar results
222 in most fields analyzed here.

223 **3. Results**

224 **3.1 Large-scale environments versus convection-centered environments**

225 Analysis using SOM with respect to MCS initiation (purple box in Fig. 1a-d) reveals four
226 types of summer MCS environments that differ substantially from one another in both the upper-
227 level circulation and surface thermodynamic conditions at the synoptic scale (Fig. 1). At 200
228 hPa, the first two types (Type-1 and Type-2) feature anomalous cyclone to the west and
229 anticyclone to the east of the MCS initiation (Fig. 1a-b). In contrast, the last two types (Type-3
230 and Type-4) show a reversed cyclone/anticyclone configuration, with anomalous anticyclone to
231 the west and cyclone to the east of the MCS initiation (Fig. 1c-d). The differences between Type-
232 1 and Type-2 are mainly the location and intensity of the anticyclone/cyclone: the intensity is
233 much stronger in Type-1; Great Plains (shown as the purple box in Fig. 1a-d) is located between
234 the anticyclone and cyclone in Type-1, while it is mainly located beneath the anticyclone in
235 Type-2. Similar differences between Type-3 and Type-4 are also found. For example, the
236 anticyclone in Type-4 is weak compared to the clear anticyclonic structure in Type-3. The upper-
237 level anticyclone has a corresponding positive surface θ_e anomaly and the upper-level cyclone
238 corresponds to a negative surface θ_e anomaly (shading in Fig. 1). The upper-level
239 anticyclone/cyclone structure in the first two types favors the initiation of MCSs by cyclonic
240 vorticity advection to the MCS initiation region, while the upper-level anticyclone/cyclone
241 structure in the last two types suppresses the initiation of MCSs by anticyclonic vorticity
242 advection to the MCS initiation region. Meanwhile, higher surface θ_e favors the initiation of

243 MCSs by destabilizing the local atmosphere, while lower surface θ_e suppresses the initiation of
244 MCSs by stabilizing the local atmosphere. Hence, the large-scale environments are generally
245 favorable for MCS initiation, especially in the warmer area of the Great Plains on the eastern
246 side of the purple box in Type-1 and on the northern side in Type-2.

247 In Type-3, although the upper-level circulation seems unfavorable for MCS initiation, the
248 wide-spread surface warmer θ_e supports MCS initiation. In Type-4, however, both upper-level
249 large-scale circulation and surface θ_e do not support MCS initiation. Hence, sub-synoptic
250 environments may play an important role in MCS initiation in Type-4. This speculation is
251 supported by the convection-centered composites shown in Fig. 1e-h. It is clear that the
252 convection-centered environments resemble the large-scale environments in the first three types,
253 but this is not the case in Type-4. In Type-4, the convection-centered composite shows an upper-
254 level cyclone to the west and anticyclone to the east of the MCS initiation location and a warmer
255 surface θ_e around the location of MCS initiation, similar to Type-1 and Type-2 except for the
256 much smaller spatial scale.

257 The GPLLJ and moisture transport are crucial in the MCS initiation. Here, we show the
258 composites of 925 hPa wind and moisture anomalies in the four types in Fig. 2. Type-1 features a
259 frontal structure, with southerly wind in the eastern Great Plains and northwesterly wind in the
260 northwestern Great Plains. As a result, positive and negative moisture anomalies occur over the
261 eastern and northwestern Great Plains, respectively (Fig. 2a). Both Type-2 and Type-3 feature
262 enhanced low-level jet and positive moisture anomalies in the northern Great Plains (Fig. 2b-c).
263 However, the enhanced jet and moisture anomalies occupy the whole northern Great Plains in
264 Type-2, but they are confined to the northwestern Great Plains in Type-3. MCSs preferentially
265 initiate in the vicinity of positive low-level moisture anomaly in the first three types. When it

266 comes to Type-4, the low-level wind anomalies are relatively weak and the Great Plains is
267 generally characterized by less moisture than normal, so the MCS initiation scatters around the
268 Great Plains and the Rocky Mountain foothills (Fig. 2d). In the convection-centered composites
269 of the low-level circulation and moisture, Type-4 is similar to all other types, with moisture
270 convergence and positive moisture anomalies around the storm initiation location (Fig. 2e-h).

271 The above large-scale environments composites based on the MCS tracking and hourly
272 ERA5 reanalysis datasets (Fig. 1a-d and Fig. 2a-d) resemble the large-scale environments
273 identified by Song et al. (2019) using 3-hourly NARR reanalysis, suggesting that the large-scale
274 environments associated with MCS initiation are robust and independent of the reanalysis
275 datasets. The convection-centered composites conducted here reveal some new features hidden
276 in the fixed-grid composites, especially for Type-3 that features an unfavorable large-scale
277 environment for MCS initiation at upper level and Type-4 that features an unfavorable large-
278 scale environment for MCS initiation at both upper level and surface. The smaller-scale cyclone
279 to the west and anticyclone to the east of MCS initiation (Fig. 1d) and the low-level moisture
280 convergence and high surface θ_e anomaly around the MCS initiation (Fig. 2h) indicate the role
281 played by sub-synoptic perturbations in Type-4.

282 The convection-centered environments are similar to the large-scale environments in the
283 first two types, but they differ substantially in Type-4, with the convection-centered
284 environments more supportive of MCS initiation than the large-scale environment. Hence, we
285 focus on the convection-centered composites in the following analysis. From a precursor
286 standpoint, it is critical to know whether the MCS initiation environments shown in Fig. 1e-h and
287 Fig. 2e-h precede the MCS initiation and thus trigger the MCSs. Figure 3 shows the convection-
288 centered environments at the same initiation location in four types except 12 hours before the

289 MCS initiation. The warm surface θ_e anomaly already occurs at the MCS initiation location even
290 12 hours before the MCS initiation, acting to destabilize the atmosphere (Fig. 3a-b). The upper-
291 level cyclone/anticyclone are also already there. The low-level wind starts to converge around
292 the initiation location and the moisture starts to increase 12 hours before the MCS initiation. It is
293 also clear that all the anomalous environmental features are more westward displaced in all the
294 four types (Fig. 3a-b vs. Fig. 1e-h; Fig. 3e-h vs. Fig. 2e-h) 12 hours earlier, indicating a possible
295 eastward propagating feature.

296 **3.2 Vertical structure of convection-centered environments**

297 In order to further examine the MCS initiation environments, we show the vertical
298 structure of convection-centered environments at the MCS initiation hour (0hr) and 12 hours
299 earlier (-12hr). Temperature and moisture fields are first examined in Fig. 4. At 0hr, moisture
300 anomalies maximize at the initiation location and larger moistening extends from the surface up
301 to 400 hPa in all the four types (Fig. 4a-b). Interestingly, the warmest temperature anomaly
302 occurs at the initiation location only in Type-3 and Type-4, but in Type-1 and Type-2, it occurs
303 about 5° east of the initiation location. In Type-1 and Type-2, although the temperature anomaly
304 at the initiation location is still positive, the magnitude is only about half of the temperature
305 maximum. Type-1 features a typical deep front, with a cold anomaly to the west and a warm
306 anomaly to the east of the initiation, but these are not that evident in Type-2. This is also
307 consistent with what we see from the spatial distribution of the Type-1 environments (Fig. 2a). In
308 Type-4, the warming is confined to the lower troposphere (below 700 hPa), but it can extend to
309 the upper troposphere (250 hPa) in the other three types. This suggests that moisture is more
310 important than temperature for the MCS initiation, no matter whether the large-scale
311 environment is favorable or not. But importantly, when the large-scale environment is not

312 favorable (i.e., Type-3 and Type-4), the local temperature becomes more important in the MCS
313 initiation, with temperature anomalies also peaking at the initiation location. The temperature
314 anomaly at -12hr is very similar to that at 0hr, except with the westward shift. Compared to 0hr,
315 the moisture field at 12hr is also positive and displaced westward, but the anomaly is broader and
316 much smaller in magnitude (note the color scale difference). This suggests that both temperature
317 and moisture anomalies favorable for the MCS initiation already exist even 12 hours before the
318 MCS initiation and may propagate eastward gradually during the 12 hours. The moisture
319 anomalies become stronger and more concentrated at the MCS initiation location due to more
320 organized mesoscale convergence (Fig. 2e-h vs. Fig. 3e-h).

321 The vertical structure of the atmospheric circulation associated with the MCS initiation
322 is shown in Fig. 5. The upper-level cyclone/anticyclone structure shown in Fig. 1e-f is roughly
323 maintained in the whole free troposphere (above 700 hPa), i.e., a cyclone to the west and an
324 anticyclone to the east of the initiation location in Type-1, Type-2 and Type-4 and an anticyclone
325 at the initiation location in Type-3. Below 700 hPa, a cyclone anomaly occurs in all the four
326 types, corresponding to the boundary layer convergence anomalies. Correspondingly, a strong
327 and narrow upward motion anomaly occurs at the initiation location, which can extend up to 150
328 hPa. The cyclone and anticyclone anomaly at -12hr has similar magnitudes compared to the
329 anomaly at 0hr, but it is westward shifted. The upward motion occurs east of the cyclone and
330 west of the anticyclone and mostly west of the initiation location, with much weaker magnitude
331 and broader area. Hence, a clear eastward propagating feature of MCS initiation environments is
332 apparent at all vertical levels, which will be further discussed in the next subsection.

333 **3.3 Eastward propagating features of MCS initiation environments**

334 As mentioned above, MCS initiation environments appear much earlier than the initiation
335 time and exhibit a gradual eastward propagation. This eastward propagating feature is more
336 apparent in the longitude-time section plots of surface variables (Fig. 6) and upper-level/low-
337 level variables (Fig. 7) along the latitude of MCS initiation. Precipitation increases rapidly after
338 the MCS initiation and propagates eastward in all four types (cyan contour in Fig. 6). This
339 reflects the propagating nature of MCSs (e.g., Carbone et al., 2002). All other variables related to
340 MCS initiation also exhibit clear eastward propagation and precede the MCS initiation in all four
341 types of large-scale environments, including the lower surface pressure and higher surface θ_e
342 (Fig. 6), anomalous cyclone and higher PV to the west and anomalous anticyclone and lower PV
343 to the east of MCS initiation location (Fig. 7a-d), as well as positive low-level moisture anomaly
344 (Fig. 7e-h) in an eastward-propagating and preceding fashion with respect to the MCS initiation.
345 Note that after the MCS initiation, stronger and faster propagating PV signals are apparent
346 (darker blue streaks in Fig. 7a-d). This propagating feature is likely related to PV generation
347 associated with the stratiform region and top-heavy latent heating profile of MCSs that
348 contribute to the longer lifetime of MCSs relative to isolated deep convection (Raymond and
349 Jiang 1990; Yang et al., 2017; Feng et al., 2018). The clear differences between the PV that
350 exists before MCS initiation and the more dominant and faster propagating PV with shorter
351 wavelength after MCS initiation underscore the role of the precursor eastward propagating
352 feature in summer MCS initiation in the Great Plains and its distinction from the PV generation
353 due to MCS rainfall.

354 Except for the low-level moisture, the propagating environments shown in Fig. 6 and Fig.
355 7 can be traced back 36 hours to 10° - 15° west of the MCS initiation in Type-1 and Type-2, 18
356 hours to around 10° west of the MCS initiation in Type-3 and 36 hours to $\sim 15^{\circ}$ west of the MCS

357 initiation in Type-4. The frontal feature is most evident in Type-1, with cold θ_e comparable to the
358 warm θ_e starting from ~ 30 hours before the MCS initiation. In the other types, the cold θ_e
359 anomaly is much smaller than the warm θ_e anomaly. The surface pressure anomaly and gradient
360 in Type-1 and Type-2 is much stronger than the other two types, supporting that the synoptic-
361 scale forcing is stronger for the first two types. The low-level moisture anomalies seem to be
362 more localized as they develop only 12 hours earlier, up to 10° west of MCS initiation, more
363 evidently in Type-3 and Type-4. This is expected considering the main source of low-level
364 moisture is confined to the Great Plains by the Rocky Mountains to the west. At the upper level,
365 the environments are modified considerably after the MCS initiation (Fig. 7a-d), possibly due to
366 the top-heavy diabatic heating from the increased stratiform precipitation associated with mature
367 MCSs, consistent with previous studies (Yang et al., 2017; Feng et al., 2018).

368 Given that the convection-centered composites shown in Fig. 7 are associated with MCS
369 initiation spanning a longitudinal range of 15° from the foothill of the Rocky Mountains to the
370 central Great Plains, the precursor environments 10° - 15° west of the convection centers (Fig. 7)
371 could be co-located with the Rocky Mountains or further upstream. To better understand the role
372 of the Rocky Mountains and regions further upstream in producing the precursor environments
373 of MCS initiation found in this study, we isolate the MCS initiation at the foothill of the Rocky
374 Mountains (35° - 50° N, 100° - 105° W) and plot the longitude-time composite of upper-level and
375 low-level environments along the latitude of MCS initiation (Fig. 8). The composite for MCS
376 initiation at the foothill (Fig. 8a-d) and that for MCS initiation across a wider range of longitudes
377 (Fig. 7a-d) show similar upper-level feature, suggesting that the propagating environments such
378 as upper-level short wave exist further upstream than the Rocky Mountains (Tuttle & Davis,
379 2013). However, the surface moisture composite of MCS initiation confining to the foothill

380 suggests that the low-level moisture only starts to accumulate shortly before the MCS initiation
381 and has no propagating feature, as is evident in Type-1 and Type-3 (Fig. 5e-h). This is mainly
382 because their sources of moisture are different: for MCS initiation at the foothill, moisture is
383 largely local while for MCS initiation over the central Great Plains (east of 100°W), moisture
384 propagates along with other dynamical environments. But at the foothill, there is not enough
385 moisture upstream to respond to the propagating waves. Hence, it is expected that the MCSs
386 initiated at the plains can produce more rainfall than those initiated at the foothill due to more
387 abundant moisture supply. This is indeed the case, as composite precipitation from MCSs
388 initiated at the Great Plains among all four types of large-scale environments is consistently
389 higher than those initiated at the foothills, particularly within the first 6 hours after initiation
390 when foothill initiated MCSs have not propagated too far away from the Rocky Mountains yet
391 (Fig. S1). These results suggest that local low-level moisture combined with a traveling wave is
392 key to the initiation of MCSs at the foothill, but over the central Great Plains (east of 100°W), it
393 is the coupling of the dynamical and moisture anomalies associated with eastward propagating
394 waves that supports MCS initiation.

395 **3.4 The role of MPs in the MCS initiation**

396 To examine the role of MPs in the MCS initiation east of the Rocky Mountains, we
397 utilize two datasets from independent MP tracking and MCS tracking to determine the likelihood
398 of co-occurrence of MPs and MCS initiation. To do this, we check whether there is an active MP
399 that spatially overlaps with the MCS cloud mask at the time of an MCS initiation. If so, we
400 consider this MCS initiation to be associated with or influenced by an MP. Based on the
401 convection-centered composites, the 600 hPa positive relative vorticity is located slightly west of
402 the center of MCS initiation (Wang et al., 2009). Accounting for this spatial relationship, an

403 active MP (initiated before this moment) found within 5° west of the MCS cloud mask at the
404 time of the MCS initiation is counted as a co-occurrence of MPs and MCS initiation.

405 Figure 9 provides more details of the calculation and the results are shown in Table 1.
406 Over the 14 years (2004-2017) analyzed, most of the MCS initiations associated with MPs occur
407 under Type-4 (over 60%), consistent with our expectation that sub-synoptic perturbations play a
408 more important role in MCS initiation in Type-4 with the weakest large-scale forcing. These 55
409 MCS initiations associated with MPs only account for less than 5% of the total MCS initiation in
410 this period (1135 MCSs in total). But considering only the 189 MPs in the 14 years, nearly 30%
411 of MPs are associated with MCS initiation. The considerable number of MPs associated with
412 MCS initiation suggests that MPs may provide a source of predictability for the Type-4 MCSs
413 (Wang et al. 2009). We next examine whether the MCSs associated with MPs are different from
414 those without MPs. We compare the probability distribution function of MCS rainfall amount,
415 rainfall area, mean rain rate and the 40 dBZ convective echo-top height between MCSs with and
416 without MPs (Fig. 10). Compared to MCSs without MPs, MCSs with MPs show lower
417 probability at low rainfall amounts/areas/rates and echo-top heights, but higher probability on the
418 high ends of rainfall amount (mainly from the stratiform rainfall amount), rainfall area (both
419 from convective and stratiform rainfall area), mean rain rate (mainly from convective rain rate)
420 and echo-top height. This suggests that MPs have a distinctively larger chance to invigorate
421 MCSs by producing more extreme rainfall over a larger area with a stronger convective activity
422 (i.e., strong winds and hail), under the weak synoptic-scale forcing associated with Type-4 MCS
423 environments.

424 **4. Conclusion and discussion**

425 In this study, self-organizing map analysis is conducted to identify four typical types of
426 propagating MCS initiation environments to better quantify the environments at the time of MCS
427 initiation, based on an MCS tracking database and the latest ERA5 reanalysis, providing data at
428 higher temporal resolution than those previously used in Song et al. (2019). We also examine the
429 relative roles of the large-scale and sub-synoptic environments in the MCS initiation for each
430 type of environments identified by the SOM analysis. These analyses highlight the crucial role of
431 propagating sub-synoptic perturbations in the MCS initiation during summer. Moreover, we
432 quantify the role of MPs in the MCS initiation over the Great Plains under unfavorable large-
433 scale environment for MCSs. The main conclusions are summarized as follows:

434 (1) The four types of MCSs identified by SOM analysis differ substantially in terms of
435 the large-scale environments. The first two types feature large-scale favorable environments in
436 the whole troposphere and surface; the large-scale environment is unfavorable at the upper-level
437 in Type-3 but favorable at the low-level and surface. The large-scale environments in Type-4
438 with negative vorticity advection and less moisture transport are most unfavorable for MCS
439 initiation. To investigate sub-synoptic factors supporting MCS initiation, we also analyze
440 convection-centered composites. The large-scale environments and convection-centered
441 environments are similar for the first three types, but they are distinct in Type-4. While Type-4
442 also features an upper-level cyclone to the west and an anticyclone to the east of MCS initiation
443 and higher θ_e near the surface similar to the features of the first two types, its circulation spatial
444 scale is much smaller. These results suggest that the MCS initiation in Type-4 is supported by
445 dynamical and thermodynamic processes similar to those of the other three types, but these
446 processes are associated with sub-synoptic perturbations instead of large-scale forcing.

447 (2) The convection-centered composites clearly show the dominance of eastward
448 propagating features prior to MCS initiation in all four types of MCS initiation environments.
449 These propagating features are clear at all vertical levels and appear much earlier (up to 36
450 hours) before the MCS initiation. Such precursors may provide some potential predictability for
451 summertime MCSs over the Great Plains. Some of the propagating perturbations originate from
452 the Rocky Mountains, while others can be traced back further west to the Pacific Northwest.
453 Both propagating environments and local, non-propagating low-level moisture are found to be
454 important in MCS initiation at the foothill of the Rocky Mountains, while in the Great Plains,
455 MCS initiation is supported by the coupled dynamical and thermodynamic propagating features.
456 Hence, the MCSs initiated at the plains can produce more rainfall than those initiated at the
457 foothill due to more abundant moisture supply.

458 (3) The role of MPs, a type of sub-synoptic perturbations under anticyclonic upper-level
459 circulation, in MCS initiation is revealed. Although less than 5% of MCS initiations are related
460 to MPs, 30% of MPs are related to MCS initiation (MPs occur much less frequently than MCSs:
461 189 vs. 1135 for 2004-2017 summer). The association of MPs with MCSs is most frequently
462 observed in Type-4 MCSs (over 60%), consistent with the understanding that under unfavorable
463 large-scale environments, sub-synoptic perturbations play a more important role in MCS
464 initiation in Type-4 than the other three types. Although MPs are only responsible for a small
465 fraction of MCS initiation, the associated Type-4 MCSs have a higher probability of producing
466 more rainfall amount, larger MCS rainfall areas, and more intense convection and rain rate than
467 those that are not associated with MPs.

468 Previous studies have identified different kinds of summer MCS initiation environments
469 both at large scale and smaller scale (e.g., Maddox, 1983; Anderson & Arritt 1998; Laing &

470 Fritsch, 2000; Coniglio et al. 2004, 2010; Peters & Schumacher, 2014; Yang et al. 2017; Song et
471 al. 2019). Eastward propagating environments have also been found by many previous studies to
472 be associated with rainfall over the Great Plains (e.g., Li & Smith 2010; Wang et al. 2011a, b;
473 Tuttle & Davis 2013; Pokharel et al., 2019). However both MCS and non-MCS storms
474 contribute similar amount of rainfall in the Great Plains so it is unclear whether and how the
475 eastward propagating environments may play a role in the summer MCS initiation. Taking
476 advantage of high spatiotemporal datasets that have only become available recently, this study
477 has filled the gap in understanding the environments for summer MCS initiation by identifying
478 the crucial role of eastward propagating environments. Further, we have quantified the
479 contribution from a specific kind of propagating environments, namely mid-tropospheric
480 perturbations. Future studies should examine contributions from other kinds of propagating
481 environments, such as shortwaves (Tuttle & Davis 2013) to the summer MCS initiation.

482 This study also shows that local, non-propagating low-level moisture anomaly is also
483 important for MCS initiation at the foothill of Rocky Mountains, but the limited spatiotemporal
484 scale may present a challenge for prediction. While such anomaly is likely related to the GPLLJ
485 moisture transport, the role of soil moisture also deserves some attention as the study region is
486 known to be a hot spot of land-atmosphere interactions (Koster et al., 2004). Remote sensing of
487 soil moisture offers a significant opportunity to advance understanding of the role of soil
488 moisture in MCS development (Klein & Taylor, 2020). Convection-permitting models are also
489 useful tools for studying MCSs. For example, we can examine whether the frequency of large-
490 scale favorable environments for MCS initiation in convection-permitting models is comparable
491 with observations, as Feng et al. (2021) noted that the frequency of large-scale favorable
492 environments is significantly underestimated in a high-resolution climate model (25-km) with

493 convection parameterization, contributing to the underestimated frequency of MCSs. As
494 convection-permitting models also need improvements in the simulation of MCSs during
495 summer compared to spring (e.g., Prein et al., 2020), an interesting question arises as to whether
496 they suffer in producing the sub-synoptic perturbations for summer MCS initiation under weak
497 large-scale environment and/or the local moisture anomaly found in this study. Advancing both
498 understanding and modeling of the precursors of MCSs and associated forcing and mechanisms
499 is important for realizing the potential of the precursors for improving prediction of summertime
500 MCSs that have significant impacts on the surface water balance (Hu et al., 2020).

501 **Acknowledgement**

502 This research is supported by the U.S. Department of Energy Office of Science Biological and
503 Environmental Research as part of the Regional and Global Climate Modeling program area.
504 PNNL is operated for the Department of Energy by Battelle Memorial Institute under contract
505 DE-AC05-76RL01830. The MCS database over the U.S. is obtained from the Department of
506 Energy Atmospheric Radiation Program (ARM): <https://doi.org/10.5439/1571643>, and the ERA5
507 dataset is obtained at <https://cds.climate.copernicus.eu/#!/search?text=ERA5&type=dataset>.

508 **References**

509 Anderson, C. J., & Arritt, R. W., (1998). Mesoscale convective complexes and persistent
510 elongated convective systems over the United States during 1992 and 1993. *Mon. Wea.*
511 *Rev.*, 126, 578–599.

512 Carbone, R. E., Tuttle, J. D., Ahijevych, D. A., & Trier, S. B., (2002). Inferences of
513 Predictability Associated with Warm Season Precipitation Episodes. *J. Atmos. Sci.*, 59, 2033–
514 2056.

515 Coniglio, M. C., Stensrud, D. J., & Richman, M. B., (2004). An observational study of derecho-
516 producing convective systems. *Wea. Forecasting*, 19, 320–337.

517 Coniglio, M. C., Hwang, J. Y., & Stensrud, D. J., (2010). Environmental factors in the upscale
518 growth and longevity of MCSs derived from rapid update cycle analyses. *Monthly Weather*
519 *Review*, 138, 3514–3539. <https://doi.org/10.1175/2010MWR3233.1>; Corrigendum, 139, 2686–
520 2688, doi:10.1175/MWR-D-11-00064.1

521 Cooney, J. W., Bowman, K. P., Homeyer, C. R., & Fenske, T. M., (2018). Ten-year analysis of
522 tropopause-overshooting convection using GridRad data, *J. Geophys. Res.*, 123, 329–343, doi:
523 10.1002/2017JD0277181.

524 Davis, C. A., Ahijevych, D. A., & Trier, S. B. (2002). Detection and Prediction of Warm Season
525 Midtropospheric Vortices by the Rapid Update Cycle, *Monthly Weather Review*, 130(1), 24-42.

526 Feng, Z. et al., (2016). More frequent intense and long-lived storms dominate the springtime
527 trend in central US rainfall. *Nat. Commun.* 7, 13429, doi:10.1038/ncomms13429.

528 Feng, Z., Leung, L. R., Houze, R. A., Hagos, S., Hardin, J., Yang, Q., Han, B., & Fan, J., (2018).
529 Structure and evolution of mesoscale convective systems: Sensitivity to cloud microphysics in

530 convection-permitting simulations over the United States. *J. Adv. Model. Earth Syst.*, 10, 1470–
531 1494.

532 Feng, Z., Houze, R. A., Leung, L. R., Song, F., Hardin, J. C., Wang, J., Gustafson, W. I., &
533 Homeyer, C. R., (2019). Spatiotemporal Characteristics and Large-Scale Environments of
534 Mesoscale Convective Systems East of the Rocky Mountains. *J. Climate*, 32, 7303–7328.

535 Feng, Z., (2019). Mesoscale convective system (MCS) database over United States, V2.
536 Atmospheric Radiation Measurement Program, accessed 1 January 2020,
537 <https://doi.org/10.5439/1571643>.

538 Feng, Z., Song, F., Sakaguchi, K., & Leung, L. R., (2021). Evaluation of Mesoscale Convective
539 Systems in Climate Simulations: Methodological Development and Results from MPAS-CAM
540 over the U.S.. *J. Climate*, 34(7), 2611-2633.

541 Gao, Y., Leung, L. R., Zhao, C., & Hagos, S., (2017). Sensitivity of summer precipitation to
542 model resolution and convective parameterizations across gray zone resolutions. *J. Geophys.*
543 *Res.*, 122, 2714-2733, doi:10.1002/2016JD025896.

544 Haberlie, A. M. & Ashley, W. S., (2019). A radar-based climatology of mesoscale convective
545 systems in the United States. *J. Climate*, 32, 1591–1606.

546 Hersbach, H., et al., (2020). The ERA5 global reanalysis. *Quart. J. Roy. Meteor. Soc.*,
547 <https://doi.org/10.1002/qj.3803>.

548 Homeyer, C. R., & Bowman, K. P., (2017). Algorithm Description Document for Version 3.1 of
549 the Three-Dimensional Gridded NEXRAD WSR-88D Radar (GridRad) Dataset, Technical
550 Report.

551 Houze, R. A., (2004). Mesoscale convective systems. *Reviews of Geophysics*, 42, RG4003.

552 Houze, R. A., (2018). 100 Years of research on mesoscale convective systems. *Meteorological*
553 *Monographs*, **59**, 17.1–17.54, <https://doi.org/10.1175/AMSMONOGRAPHS-D-18-0001.1>.

554 Hu, H., Leung, L. R., & Feng, Z., (2020). Understanding the distinct impacts of MCS and non-
555 MCS rainfall on the surface water balance in the central U.S. using a numerical water-tagging
556 technique. *J. Hydrometeor.*, doi:10.1175/JHM-D-20-0081.1.

557 Huang, X., Hu, C., Huang, X. et al. A long-term tropical mesoscale convective systems dataset
558 based on a novel objective automatic tracking algorithm. *Clim Dyn* 51, 3145–3159 (2018).
559 <https://doi.org/10.1007/s00382-018-4071-0>.

560 Janowiak, J., Joyce, B., & Xie, P., (2017). NCEP/CPC L3 Half Hourly 4km Global (60S - 60N)
561 Merged IR V1, edited by Andrey Savtchenko, Greenbelt, MD, Goddard Earth Sciences Data and
562 Information Services Center (GES DISC), Accessed: [**1 February**
563 **2018**], [10.5067/P4HZB9N27EQU](https://doi.org/10.5067/P4HZB9N27EQU).

564 Johns, R. H., (1982). A synoptic climatology of northwest flow severe weather outbreaks. Part I:
565 nature and significance. *Mon. Weather Rev.*, 110, 1653–1663.

566 Johns, R. H., (1984). A synoptic climatology of northwest flow severe weather outbreaks. Part II:
567 meteorological parameters and synoptic patterns. *Mon. Weather Rev.*, 112, 449–464.

568 Johns R. H., (1993). Meteorological conditions associated with bow echo development in
569 convective storms. *Weather Forecast*, 8, 294–299.

570 Koster, R.D., et al., (2004). Regions of strong coupling between soil moisture and precipitation.
571 *Science*, 305, 1138, doi:10.1126/science.1100217.

572 Klein, C., & Taylor, C. M., (2020). Dry soils can intensify mesoscale convective systems. *Proc.*
573 *Nat. Acad. Sci.*, 117 (35), 21132-21137, doi:10/1073/pnas.2007998117.

574 Laing, A. G. & Fritsch, J. M., (2000). The large scale environments of the global populations of
575 mesoscale convective complexes. *Mon. Weather Rev.* 128, 2756–2776.

576 Li, Y., & Smith, R. B., (2010). The detection and significance of diurnal pressure and potential
577 vorticity anomalies east of the Rockies. *J. Atmos. Sci.*, 67, 2734–2751.

578 Lin, Y., (2011). GCIP/EOP Surface: Precipitation NCEP/EMC 4KM Gridded Data (GRIB) Stage
579 IV Data. Version 1.0. UCAR/NCAR - Earth Observing Laboratory.
580 <https://doi.org/10.5065/D6PG1QDD>. Accessed Nov 2017.

581 Lin, Y., Dong, W., Zhang, M., Xie, Y., Xue, W., Huang, J., & Luo, Y. (2017). Causes of model
582 dry and warm bias over central U.S. and impact on climate projections. *Nature Communications*,
583 8(1), 881. <https://doi.org/10.1038/s41467-017-01040-2>.

584 Ma, H.-Y., Klein, S. A., Xie, S., Zhang, C., Tang, S., Tang, Q., et al., (2018). CAUSES: On the
585 Role of Surface Energy Budget Errors to the Warm Surface Air Temperature Error Over the
586 Central United States. *Journal of Geophysical Research: Atmospheres*, 123(5), 2888-2909.
587 <https://agupubs.onlinelibrary.wiley.com/doi/abs/10.1002/2017JD027194>.

588 Maddox, R. A., Chappell, C. F., & Hoxit, L. R., (1979). Synoptic and meso- α -scale aspects of
589 flash flood events. *Bull. Amer. Meteor. Soc.*, 60, 115–123, doi:10.1175/1520-0477-60.2.115.

590 Maddox, R. A., (1983). Large-scale meteorological conditions associated with midlatitude,
591 mesoscale convective complexes. *Monthly Weather Review*, 111(7), 1475–1493.

592 Mesinger, F., and Coauthors, (2006). North American Regional Reanalysis. *Bulletin of the*
593 *American Meteorological Society*, **87**, 343-360.

594 Peters, J. M., & Schumacher, R. S., (2014). Objective categorization of heavy-rain-producing
595 MCS synoptic types by rotated principal component analysis. *Monthly Weather Review*, 142(5),
596 1716-1737.

597 Pokharel, B., Wang, S. Y., Meyer, J., Gillies, R., & Lin, Y., (2019). Climate of the weakly-
598 forced yet high-impact convective storms throughout the Ohio River Valley and Mid-Atlantic
599 United States. *Clim. Dyn.*, 52, 5709–5721.

600 Prein, A.F., Liu, C., Ikeda, K., et al., (2020). Simulating North American mesoscale convective
601 systems with a convection-permitting climate model. *Clim. Dyn.*, 55, 95–110.
602 <https://doi.org/10.1007/s00382-017-3993-2>

603 Raymond, D. J., & Jiang, H., (1990). A theory for long-lived mesoscale convective systems. *J.*
604 *Atmos. Sci.*, 47(24), 3067-3077.

605 Schumacher, R. S., & Johnson, R. H., (2005). Organization and environmental properties of
606 extreme-rain-producing mesoscale convective systems. *Mon. Wea. Rev.*, 133, 961–976.

607 Schumacher, R. S., & Johnson, R. H., (2006). Characteristics of U.S. extreme rain events during
608 1999–2003. *Wea. Forecasting*, 21, 69–85.

609 Stein, T. H. M., Hogan, R. J., Hanley, K. E., Nicol, J. C., Lean, H. W., Plant, R. S., Clark, P. A.,
610 & Halliwell, C. E. (2014). The Three-Dimensional Morphology of Simulated and Observed
611 Convective Storms over Southern England, *Monthly Weather Review*, 142(9), 3264-3283.

612 Trier, S. B., Davis, C. A., Ahijevych, D. A., Weisman, M. L., & Bryan, G. H., (2006).
613 Mechanisms Supporting Long-Lived Episodes of Propagating Nocturnal Convection within a 7-
614 Day WRF Model Simulation. *J. Atmos. Sci.*, 63, 2437–2461.

615 Tuttle, J. D., & Davis, C. A., (2013). Modulation of the Diurnal Cycle of Warm-Season
616 Precipitation by Short-Wave Troughs. *J. Atmos. Sci.*, 70, 1710–1726.

617 Wang, S., Chen, T., & Taylor, S. E., (2009). Evaluations of NAM Forecasts on Midtropospheric
618 Perturbation-Induced Convective Storms over the U.S. Northern Plains. *Wea. Forecasting*, 24,
619 1309–1333, <https://doi.org/10.1175/2009WAF2222185.1>.

620 Wang, S., Chen, T. C., & Correia, J., (2011a). Climatology of summer midtropospheric
621 perturbations in the US northern plains. Part I: Influence on northwest flow severe weather
622 outbreaks. *Clim. Dyn.*, 36, 793–810.

623 Wang S., Chen, T. C., & Takle, E. S., (2011b). Climatology of summer midtropospheric
624 perturbations in the US northern plains. Part II: Large-scale effects of the Rocky Mountains on
625 genesis. *Clim. Dyn.*, 36, 1221–1237.

626 Yang, Q., Houze, R. A., Leung, L. R., & Feng, Z., (2017). Environments of long-lived mesoscale
627 convective systems over the central United States in convection permitting climate
628 simulations. *J. Geophys. Res. Atmos.*, 122, 13 288–13 307.

629 **Table captions**

630 **Table 1** The MCS number in each type, total MP number and the number of overlaps between
631 MCS and MP in each type for 2004-2017 summer (June-July-August). The percentage of
632 overlaps to the total MCS number in each type is also shown in the bracket.

633 **Figure captions**

634 **Fig. 1** (a-d) Composite anomalies of 200 hPa geopotential height (contour; units: m) and surface
635 equivalent potential temperature (shading; units: K) during June-July-August (JJA) in each type
636 of large-scale environment determined by the SOM analysis. The anomalies are relative to all
637 times during JJA. The percentage in the upper right corner indicates the percentage of occurrence
638 of each environment type. The solid (dashed) lines represent positive (negative) 200 hPa
639 geopotential height anomalies, with an interval of 5 m. (e-h) The same as (a-d) but for
640 convection-centered composites. The purple and black boxes in (a-d) indicate the boundaries of
641 MCS initiation over the Great Plains (25°-50°N, 90°-105°W) and the SOM analysis domain (20°
642 -55°N, 70°-110°W), respectively. The cyan dots denote the location of MCS initiation. The
643 purple dot in (e-h) indicates the MCS initiation location (0°, 0°); E (W) in the x-axis means east
644 (west) of the convection initiation and N (S) in the -axis means north (south) of the convection
645 initiation.

646 **Fig. 2** Same as Fig. 1 but for 925 hPa wind (vector; units: m s⁻¹) and specific humidity (shading;
647 units: g kg⁻¹). The grey contour in (a-d) shows elevation higher than 1500 m based on the
648 TBASE data.

649 **Fig. 3** The convection-centered composite anomalies of (top panel) 200 hPa geopotential height
650 (contour; units: m) and surface equivalent potential temperature (shading; units: K), and (bottom
651 panel) 925 hPa wind (vector; units: m s⁻¹) and specific humidity (shading; units: g kg⁻¹) at the 12
652 hours before the MCS initiation during June-July-August (JJA) in each type of large-scale
653 environment determined by the SOM analysis. The purple dot indicates the MCS initiation
654 location (0°, 0°); E (W) in the x-axis means east (west) of the convection initiation and N (S) in
655 the y-axis means north (south) of the convection initiation.

656 **Fig. 4** Longitude-height cross-sections of specific humidity (shading; units: g kg^{-1}) and
657 temperature (contour; units: K) in the convection-centered composites in the four types at the
658 initiation hour (top panel) and 12 hours before the initiation (bottom panel). Purple line shows
659 the initiation location. E (W) in the x-axis means east (west) of the convection initiation. The
660 contour interval is 0.3 K and the bold line is the zero contour.

661 **Fig. 5** Same as Fig. 4 but for vertical velocity (shading; units: $10^{-2} \text{ Pa s}^{-1}$) and geopotential height
662 (contour; units: m). The contour interval is 3 m.

663 **Fig. 6** The longitude-time section of convection-centered environments along the latitude of
664 MCS initiation spanning from the foothill of the Rocky Mountains to the central Great Plains (25
665 $^{\circ}$ - 50° N, 90° - 105° W; purple boxes in Fig.1a-d and Fig. 2a-d): surface equivalent potential
666 temperature (shading; units: K), surface pressure (black contour; units: hPa) and precipitation
667 (cyan contour; units: mm day^{-1}). The black solid (dashed) lines represent positive (negative)
668 surface pressure, with an interval of 0.3 hPa. The solid cyan lines represent positive precipitation,
669 with an interval of 0.3 mm/day. The purple dot indicates the MCS initiation longitude and
670 moment (0° and 0 hr); E (W) in the x-axis means east (west) of the convection initiation and +
671 (-) in the y-axis means after (before) the convection initiation.

672 **Fig. 7** The longitude-time section of convection-centered environments along the latitude of
673 MCS initiation spanning from the foothill of the Rocky Mountains to the central Great Plains (25
674 $^{\circ}$ - 50° N, 90° - 105° W; purple boxes in Fig.1a-d and Fig. 2a-d): (a-d) 200 hPa potential vorticity
675 (shading; units: $10^{-6} \text{ K m}^2 \text{ kg}^{-1} \text{ s}^{-1}$) and geopotential height (contour: units: m) and (e-h) 925 hPa
676 specific humidity (units: g kg^{-1}). In (a-d), the black solid (dashed) lines represent positive
677 (negative) geopotential height, with an interval of 3 m. The purple dot indicates the MCS

678 initiation longitude and moment (0° and 0 hr); E (W) in the x-axis means east (west) of the
679 convection initiation and + (-) in the y-axis means after (before) the convection initiation.

680 **Fig. 8** Same as Fig. 4 but for MCSs initiated at the foothill of Rocky Mountain (35° - 50° N; 100° -
681 105° W).

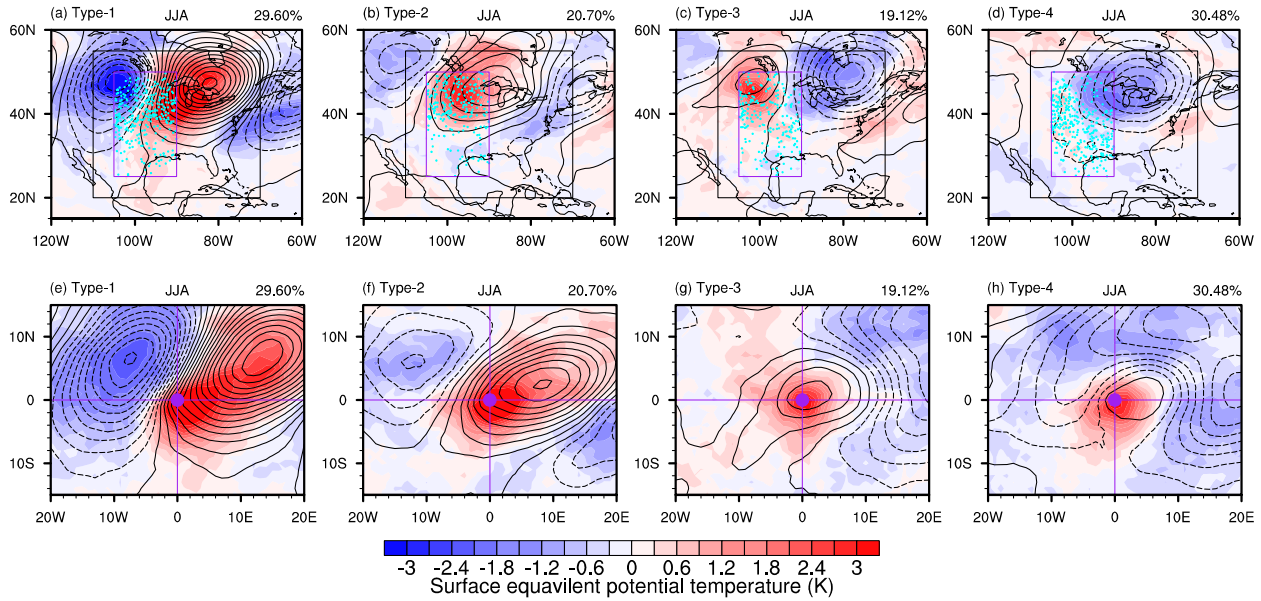
682 **Fig. 9** Schematic plot of the calculation of overlap between mid-tropospheric perturbation (MP)
683 and MCS based on their respective tracking records. The different colors in this map show the
684 different numbers assigned to each MCS at initiation (shown as cloud numbers). The highest
685 number of 281 is for MCSs initiated at the presented time (2009-07-30-Z01). At the moment of
686 MCS initiation, we search the MP tracking record for a spatial overlap between the new MCS
687 and an active MP (the MP should be initiated before this moment). The spatial extent of each MP
688 is represented by the blue square based on the center coordinate and areal coverage (in terms of
689 the number of the ERA5 grid points) provided by the MP tracking algorithm (circular shape is
690 also tested and gives the same results). As the MP has a threshold and the grid points with lower
691 values are not labeled as MP, the MP area coverage is doubled (we also tested even larger area,
692 but the results are unchanged) to consider the potential impacts of these lower values on the
693 MCS initiation.

694 **Fig. 10** Probability distribution function (PDF) of (a) MCS rainfall amount (units: 10^4 mm hr⁻¹),
695 (b) MCS rainfall area (units: 10^4 km²), (c) MCS rain rate (units: mm hr⁻¹) and (d) 40 dBZ echo
696 top height (units: km) in Type-4 with (blue bar) and without (red bar) MPs.

697 **Table 1** The MCS number in each type of large-scale environments, the total MP number and
 698 the number of overlaps between MCS initiations and MPs in each type for 2004-2017 summer
 699 (June-July-August). The percentage of overlaps in the total MCS number in each type is also
 700 shown in the bracket.

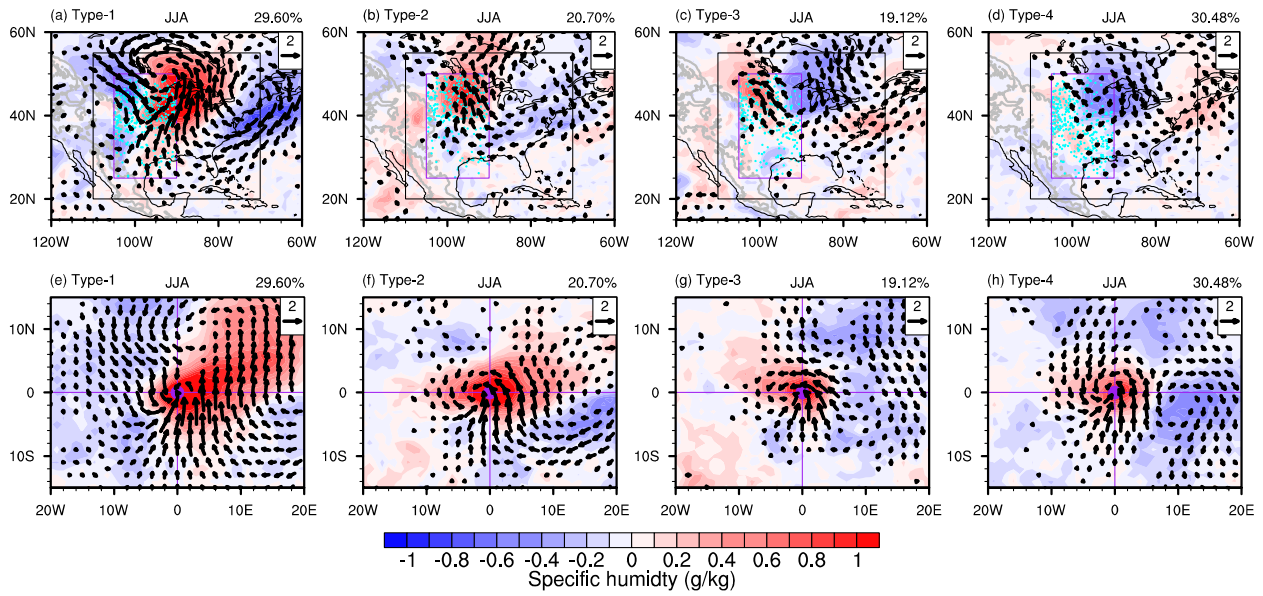
	Type-1	Type-2	Type-3	Type-4
MCS number	336	235	217	347
MP number	189			
MCS overlap with MP	9 (2.7%)	7 (3.0%)	5 (2.3%)	34 (10%)

701



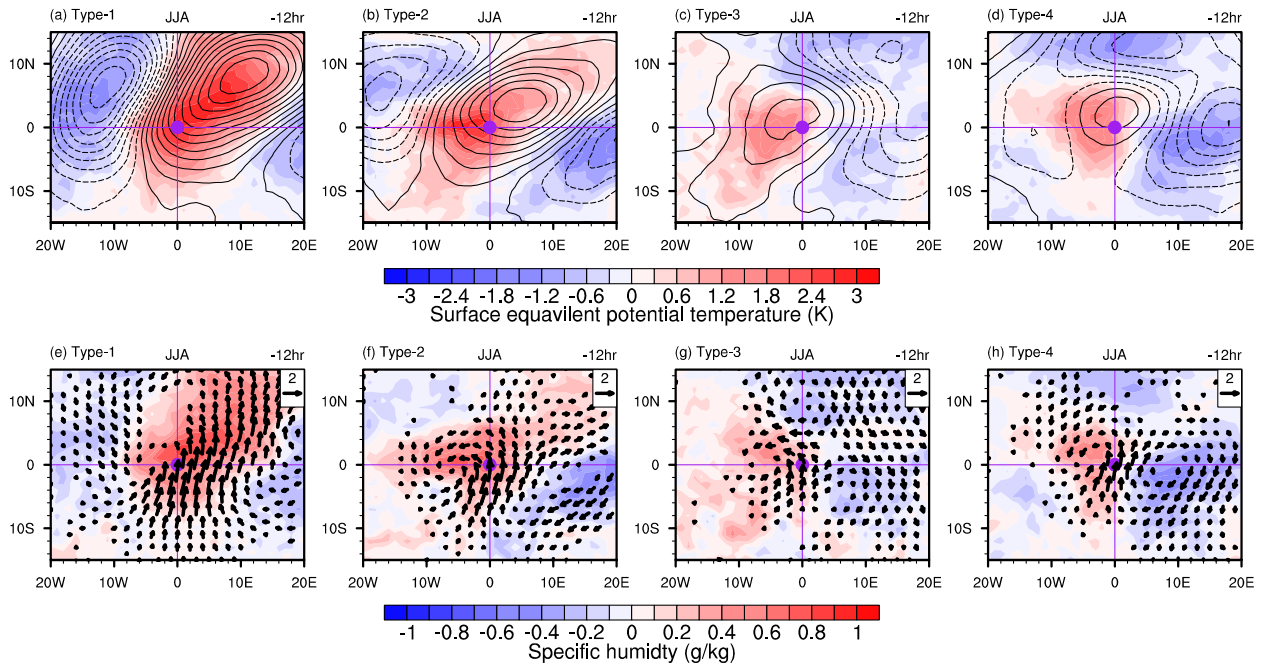
702

703 **Fig. 1** (a-d) Composite anomalies of 200 hPa geopotential height (contour; units: m) and surface
 704 equivalent potential temperature (shading; units: K) during June-July-August (JJA) in each type
 705 of large-scale environment determined by the SOM analysis. The anomalies are relative to all
 706 times during JJA. The percentage in the upper right corner indicates the percentage of occurrence
 707 of each environment type. The solid (dashed) lines represent positive (negative) 200 hPa
 708 geopotential height anomalies, with an interval of 5 m. (e-h) The same as (a-d) but for
 709 convection-centered composites. The purple and black boxes in (a-d) indicate the boundaries of
 710 MCS initiation over the Great Plains (25° - 50° N, 90° - 105° W) and the SOM analysis domain (20°
 711 -55° N, 70° - 110° W), respectively. The cyan dots denote the location of MCS initiation. The
 712 purple dot in (e-h) indicates the MCS initiation location (0° , 0°); E (W) in the x-axis means east
 713 (west) of the convection initiation and N (S) in the -axis means north (south) of the convection
 714 initiation.



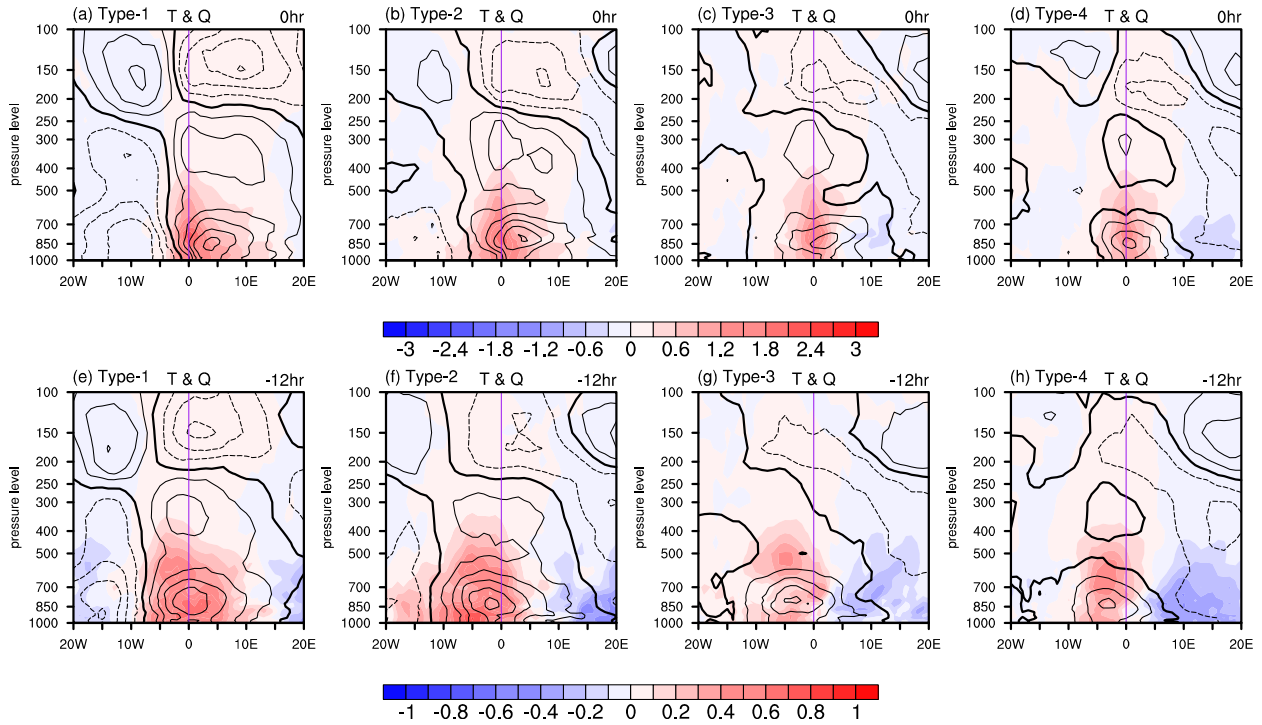
715

716 **Fig. 2** Same as Fig. 1 but for 925 hPa wind (vector; units: m s^{-1}) and specific humidity (shading;
 717 units: g kg^{-1}). The grey contour in (a-d) shows elevation higher than 1500 m based on the
 718 TBASE data. The vector with wind speed smaller than 0.2 m s^{-1} is omitted.



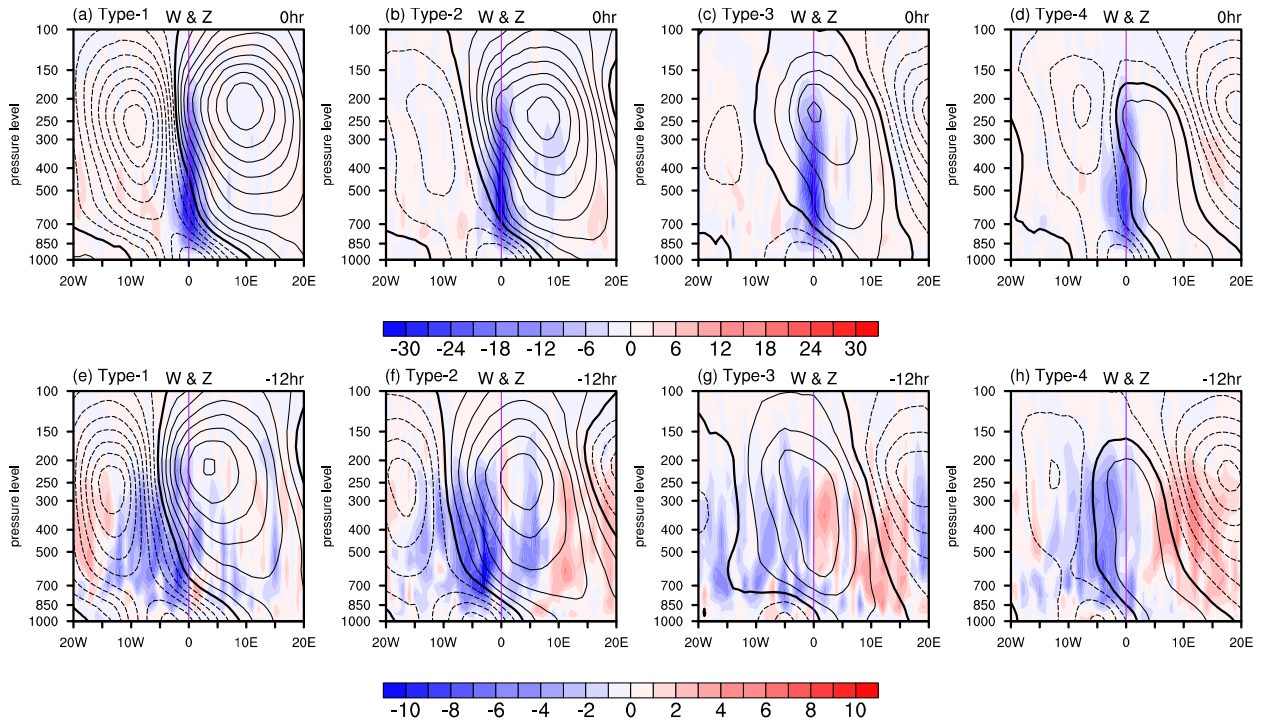
719

720 **Fig. 3** The convection-centered composite anomalies of (top panel) 200 hPa geopotential height
 721 (contour; units: m) and surface equivalent potential temperature (shading; units: K), and (bottom
 722 panel) 925 hPa wind (vector; units: m s^{-1}) and specific humidity (shading; units: g kg^{-1}) at the 12
 723 hours before the MCS initiation during June-July-August (JJA) in each type of large-scale
 724 environment determined by the SOM analysis. The purple dot indicates the MCS initiation
 725 location ($0^\circ, 0^\circ$); E (W) in the x-axis means east (west) of the convection initiation and N (S)
 726 the y-axis means north (south) of the convection initiation. The vector with wind speed smaller
 727 than 0.2 m s^{-1} is omitted.



728

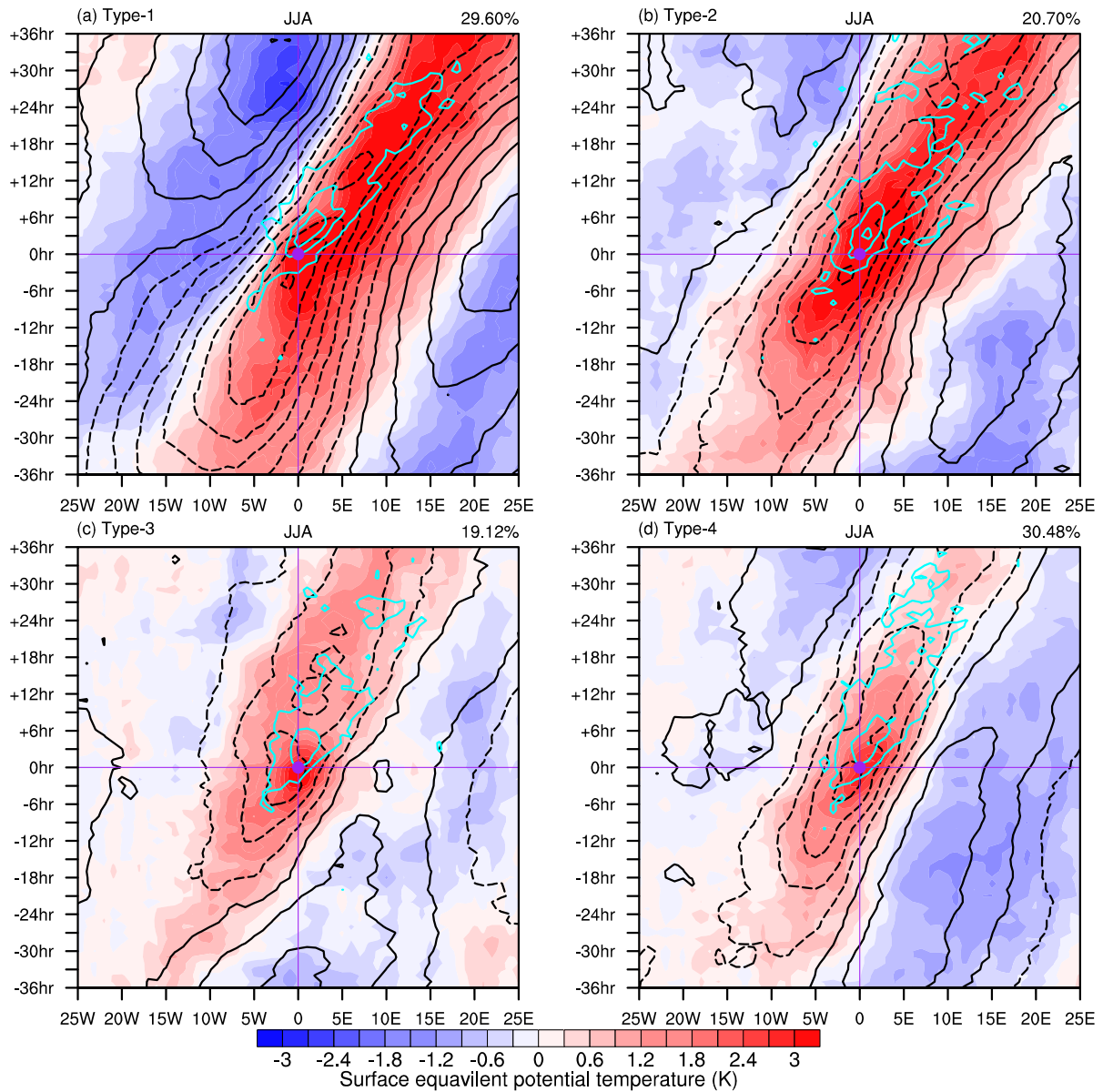
729 **Fig. 4** Longitude-height cross-sections of specific humidity (shading; units: g kg^{-1}) and
 730 temperature (contour; units: K) in the convection-centered composites in the four types at the
 731 initiation hour (top panel) and 12 hours before the initiation (bottom panel). Purple line shows
 732 the initiation location. E (W) in the x-axis means east (west) of the convection initiation. The
 733 contour interval is 0.3 K and the bold line is the zero contour.



734

735 **Fig. 5** Same as Fig. 4 but for vertical velocity (shading; units: $10^{-2} \text{ Pa s}^{-1}$) and geopotential height

736 (contour; units: m). The contour interval is 3 m.

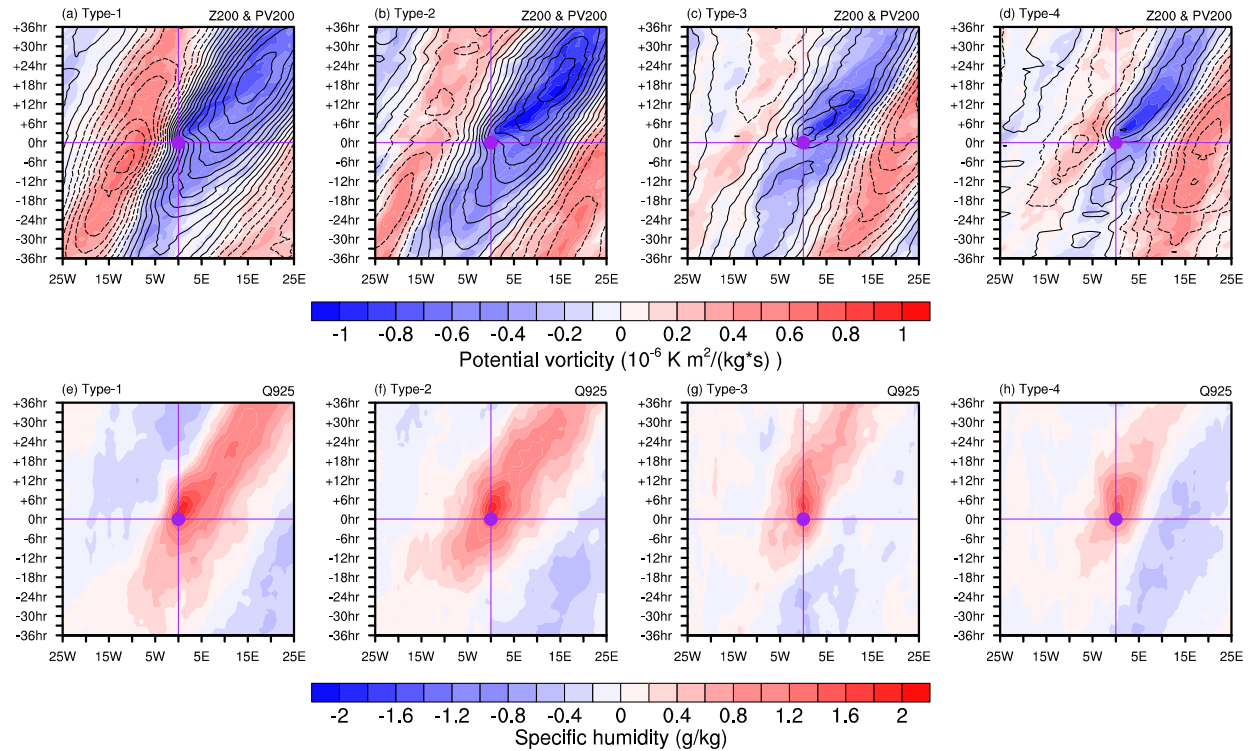


737

738 **Fig. 6** The longitude-time section of convection-centered environments along the latitude of
 739 MCSs initiation spanning from the foothill of the Rocky Mountains to the central Great Plains
 740 (25°-50°N, 90°-105°W; purple boxes in Fig.1a-d and Fig. 2a-d): surface equivalent potential
 741 temperature (shading; units: K), surface pressure (black contour; units: hPa) and precipitation
 742 (cyan contour; units: mm day⁻¹). The black solid (dashed) lines represent positive (negative)
 743 surface pressure, with an interval of 0.3 hPa. The solid cyan lines represent positive precipitation,

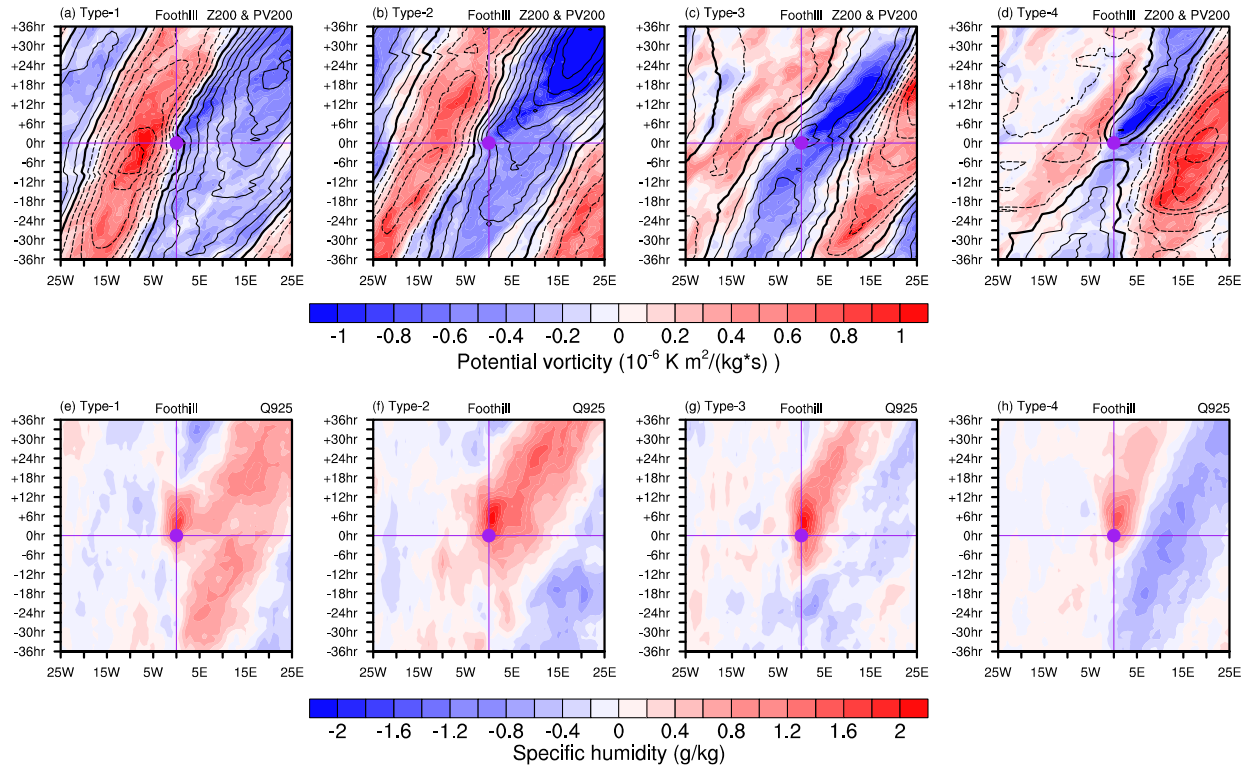
744 with an interval of 0.3 mm/day. The purple dot indicates the MCS initiation longitude and
745 moment (0° and 0 hr); E (W) in the x-axis means east (west) of the convection initiation and +
746 (-) in the y-axis means after (before) the convection initiation.

747



748

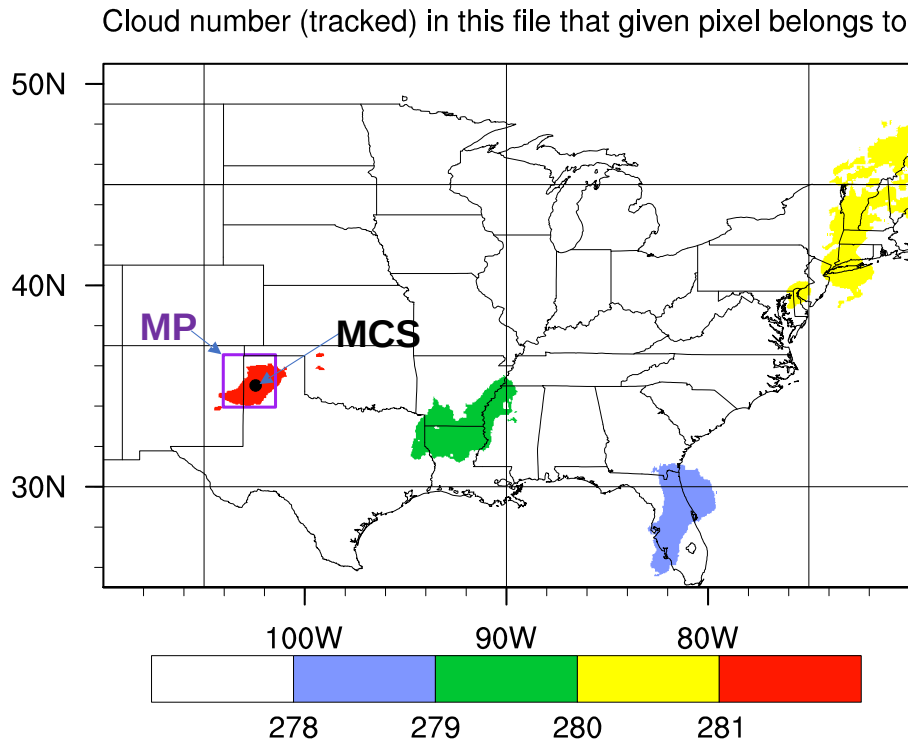
749 **Fig. 7** The longitude-time section of convection-centered environments along the latitude of
 750 MCSs initiation spanning from the foothill of the Rocky Mountains to the central Great Plains
 751 (25° - 50° N, 90° - 105° W; purple boxes in Fig. 1a-d and Fig. 2a-d): (a-d) 200 hPa potential vorticity
 752 (shading; units: 10^{-6} K m² kg⁻¹ s⁻¹) and geopotential height (contour: units: m) and (e-h) 925 hPa
 753 specific humidity (units: g kg⁻¹). In (a-d), the black solid (dashed) lines represent positive
 754 (negative) geopotential height, with an interval of 3 m. The purple dot indicates the MCS
 755 initiation longitude and moment (0° and 0 hr); E (W) in the x-axis means east (west) of the
 756 convection initiation and + (-) in the y-axis means after (before) the convection initiation.



757

758 **Fig. 8** Same as Fig. 7 but for MCSs initiated at the foothill of Rocky Mountain (35° - 50° N; 100° -
 759 105° W).

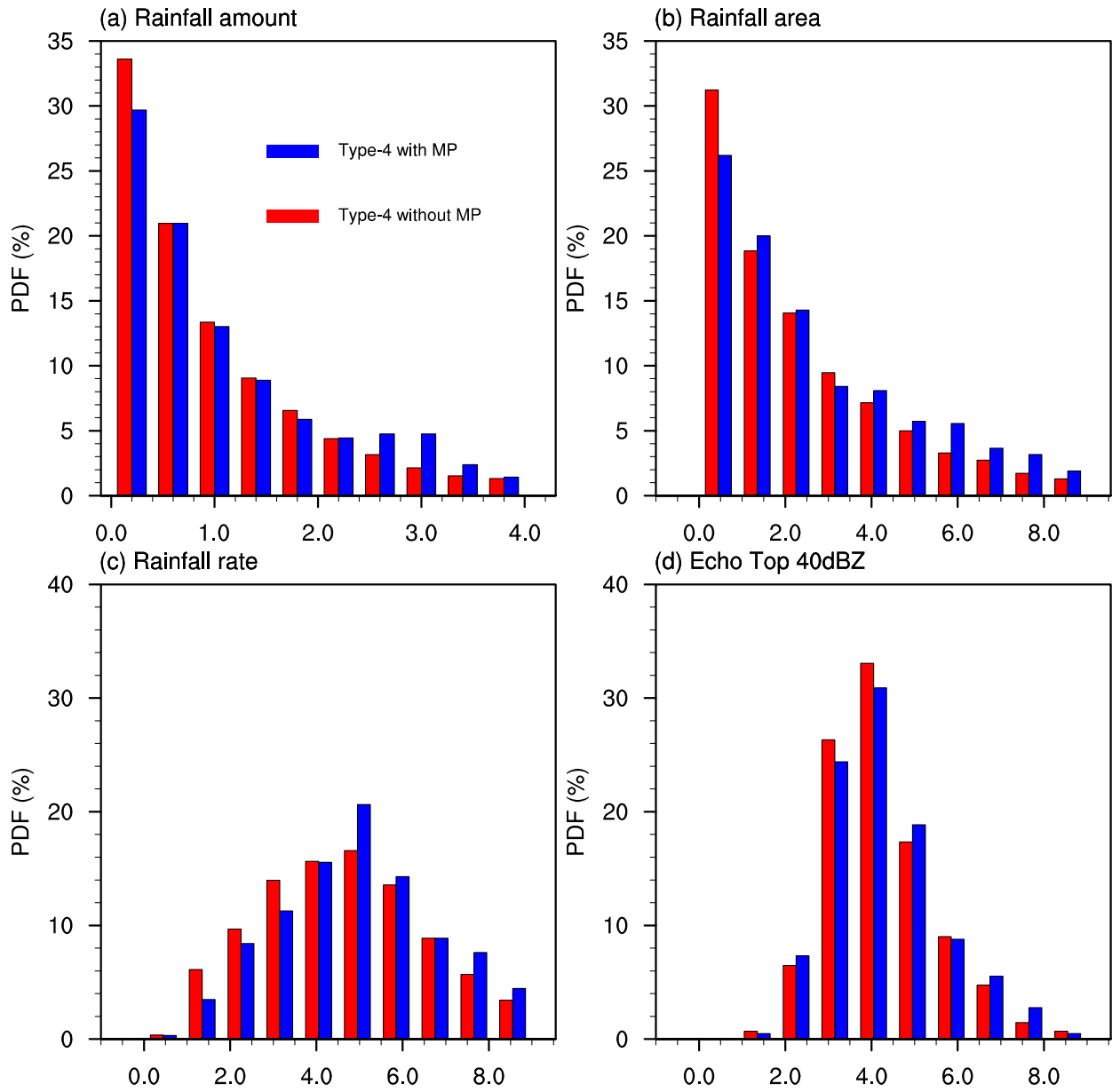
The overlap between MP and MCS at 2009073001



760

761 **Fig. 9** Schematic plot of the calculation of overlap between mid-tropospheric perturbation (MP)
762 and MCS based on their respective tracking records. The different colors in this map show the
763 different numbers assigned to each MCS at initiation (shown as cloud numbers). The highest
764 number of 281 is for MCSs initiated at the presented time (2009-07-30-Z01). At the moment of
765 MCS initiation, we search the MP tracking record for a spatial overlap between the new MCS
766 and an active MP (the MP should be initiated before this moment). The spatial extent of each MP
767 is represented by the blue square based on the center coordinate and areal coverage (in terms of
768 the number of the ERA5 grid points) provided by the MP tracking algorithm (circular shape is
769 also tested and gives the same results). As the MP has a threshold and the grid points with lower
770 values are not labeled as MP, the MP area coverage is doubled (we also tested even larger area,
771 but the results are unchanged) to consider the potential impacts of these lower values on the
772 MCS initiation.

46



773

774 **Fig. 10** Probability distribution function (PDF) of (a) MCSs rainfall amount (units: 10^4 mm hr⁻¹),

775 (b) MCSs rainfall area (units: 10^4 km²), (c) MCSs rainfall rate (units: mm hr⁻¹) and (d) echo top

776 40 dBZ (units: km) in Type-4 with MP (blue bar) and Type-4 without MP (red bar).